Synthesis of Nanosize Powders and Thin Films of Yb-Doped YAG by Sol−Gel Methods

H. M. Wang,* M. C. Simmonds, Y. Z. Huang, and J. M. Rodenburg

Materials Research Institute, Sheffield Hallam University, City Campus, Sheffield S1 1WB, U.K.

Received July 2, 2002. Revised Manuscript Received June 2, 2003

Yb-doped YAG is becoming a very promising optical material. We present a synthesis of single-phase Yb-doped YAG powders and thin films at a significantly lower temperature by sol−gel methods than by other conventional techniques. Yb-doped YAG powders and thin films on Si(100) substrates with a series of different doping concentrations were prepared. The lattice deformation, IR, and Raman vibrations were studied via the change of the doped concentration. This could be one of the reasons why, in general, about 20 atomic % Yb:YAG presents the better laser and scintillation properties. Scanning electron microscopy and transmission electron microscopy were used to investigate the morphology of the structures. A strong preferred orientation of crystal growth in thin films was found during the conversion of the structure from amorphous to crystalline. The Avrami model was used to analyze the isothermal transformation kinetics. On the basis of the experimental results, the effective activation energy of crystallization in the thin films was calculated as 653 ± 10 kJ/mol.

1. Introduction

$Y_3Al_5O_{12}$ (YAG) has excellent thermal properties and is well established as a laser host material.[1] Conventionally, these materials such as Nd- or Cr-doped YAG are single crystals fabricated by the Czochralski (CZ) method.[2] The schematic diagram of the CZ method, also called a "puller", is shown in Figure 1. Such a puller generally has four subsystems, which are the furnace, pulling mechanism, gas control, and control system. The high-purity raw materials are melted at extremely high temperature (2000 °C). The growth of a single crystal is very sluggish. Heavily doped Nd:YAG crystals (<5 atomic %) are necessary for obtaining a high-power output laser. However, in general, it is extremely difficult to dope more than 1 atomic % Nd homogeneously in a YAG single crystal because the effective segregation coefficient[3] of Nd for the YAG single crystals is quite low (∼0.2). YAG single crystals doped with more than 2 atomic % of elemental Nd have a relatively inferior optical quality that cannot be used as laser devices. Thus, in recent years, ceramic laser materials have received much attention.[4−8] Especially with the development of nanomaterials, it has become possible to produce transparent high-quality ceramics of YAG by the isostatically pressed method. It has been reported[8] that a high optical quality Nd:YAG ceramic presents almost the same laser property as the single-crystal rod lately. Compared to single-crystal growth, the technique of manufacturing ceramics offers the advantages of being inexpensive and having an easy high-doped concentration, mass production, large size, and gradient ceramic structure. Furthermore, we noticed that Yb-doped YAG has recently been suggested as a new-generation laser medium.[9,10] It is attractive for Q-switching operations to obtain high-peak-power

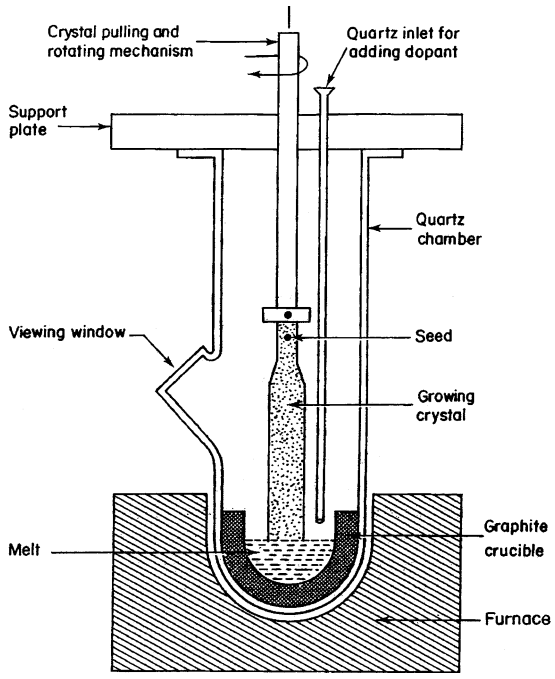

Figure 1. Schematic representation of a CZ crystal pulling furnace.

(1) Zayhowski, J. J. *J. Alloys Compd.* **2000**, *303−304*, 393.
(2) Kvapil, J.; et al. *J. Cryst. Growth* **1981**, *52*, 542.
(3) Shiroki, K. *Solid-state Laser Mater. Oyobutsuri* **1969**, *38*, 117.
(4) Sekita, M.; et al. *J. Appl. Phys.* **1990**, *67*, 453.
(5) Ikesue, A.; Furusato, I.; et al. *J. Am. Ceram. Soc.* **1995**, *78* (1), 225.
(6) Ikesue, A. *Opt. Mater.* **2002**, *19*, 183−187.
(7) Hreniak, D.; Strek, W. *J. Alloys Compd.* **2002**, *341*, 183−186.
(8) Lu, J. R.; Uede, K.; Yagi, H.; Yanagitani, T.; Akiyama, Y.; Kaminskii, A. A. *J. Alloys Compd.* **2002**, *341*, 220−225.
(9) Shimokozono, M.; Sugimoto, N.; et al. *Appl. Phys. Lett.* **1996**, *68*, 2177.

10.1021/cm021248l CCC: $25.00
Published on Web 08/09/2003

optical pulses[11,12] because it has relatively low cross-sections that lead to larger pulse energies (4 times higher) compared with those of Nd-doped crystals. Heavily Yb-doped YAG is also found to be a potentially good scintillator for solar neutrino detection very recently and can be optimized in terms of efficiency and lifetime.[13,14] The laser and scintillation properties of Yb-doped YAG with a doped concentration from 1 to 100% are being widely studied.[14−19] However, the optical properties of Yb:YAG materials have been significantly affected with the increase of the doped Yb^{3+} concentration in Yb:YAG due to the crystal lattice deformation and the adjustment of the lattice constant. This is attributed to the change of the phonon vibration modes. These properties are important to the design of the system of laser devices, but very little research about these properties can be found.

Here, we report the manufacturing of Yb:YAG powders with different doping concentrations from low to high by sol−gel methods. The change in the phonon vibration IR and Raman spectra was studied. The sol−gel way has many advantages such as atomic level mixing of high-purity precursors and low processing temperature. Nanosize particles are very significant in preparing high-quality ceramics. Although a lot of sol−gel or similar chemical syntheses of the pure YAG[20−22] and doped YAG (mainly Ce^{3+}, Eu^{3+}, and Tb^{3+}) powders were reported recently, most of them are used as phosphors and the doped concentration is normally lower than 5%. To the best of our knowledge, we are the first to synthesize the heavily Yb-doped YAG material by the sol−gel method.

2. Experimental Section

Al sol was prepared first from $AlCl_3$ (99.985%, Alfa), and then the yttrium and ytterbium chemicals were added to the Al sol. The molar ratio of Yb:Y was controlled to 10%, 20%, 50%, and 100%. The ratio of (Yb + Y):Al was kept as 3:5. After several hours of mixing at 80 °C, a clear transparent sol was obtained. Details can be found in ref 23.

The gel for the preparation of Yb:YAG powders was formed by putting dropwise the clear sol into the 35 wt % NH_4OH solution that is stirred continually. The ammonia solution became opaque because of the formation of gel. Then, the suspension solution was filtered, and the residue gel was dried at 200 °C for about 1 or 2 h to get a white powder and further heat-treated in air at the crystallized temperature with a heating rate of 10 °C min^{-1}.

Thin films were deposited on the substrate of single-crystal Si(100) by dip coating, and the specimens were cut into pieces of 1 × 1 cm^2. The thickness of the film was under 1 μm. The thin film samples were calcined separately at 850, 900, and 950 °C for various times with a very fast heating rate of 100 °C s^{-1}. A ramp rate of 100 °C s^{-1} was sufficiently fast to prevent transformation during heating and allowed the direct application of a JMA model[24−27]− for transformation kinetics.

X-ray diffraction (XRD) patterns of powders and thin films of Yb:YAG were characterized using a Philips PW-3710 diffractometer equipped with Cu Kα radiation. The tube current and voltage were 35 mA and 35 kV, respectively. The scan step time was 4 s, and the step size was 0.020. The 2θ range examined was 15−60°. Disk samples for the experiment of infrared transmittance spectra were prepared by mixing Yb:YAG powders with KBr according to the mass ratio 10:100. Infrared spectra of Yb:YAG powders were performed in a Genesis series Fourier transform infrared (FT-IR) made by ATI Mattson, and Raman spectra were finished in a Renishaw Ramanscope system 2000 spectrometer using the helium/neon laser with a laser wavelength of 633 nm and 25 mW power. The examined wavenumber range of IR is from 1000 to 400 cm^{-1}. For Raman spectra, it is in the range of 200−1000 cm^{-1}.

The surface morphology of powders was investigated using XL30 ESEM-FEG. Specimens for transmission electron microscopy (TEM) observation were prepared by briefly dispersing ultrasonically the powders in acetone. One drop of the solution was then placed on a copper grid coated with an evaporated amorphous carbon film. TEM characterization was performed on a Philips CM20 at 200 kV.

3. Results and Discussion

3.1. Crystalline Structure Conversion. 3.1.1. The powders annealed at 800 °C were found to be amorphous, with small crystallites whose size was in the nanoscale. However, the fully crystallized phase was identified as a garnet structure for powders after being heated at 850 °C (JCPDS[28] No. 33-40 for YAG and No. 73-1369 for YbAG). Traditionally, the synthesis temperature high up to 1600 °C is required by solid-state sintering methods. The XRD patterns are shown in Figure 2 A−D respectively for 10, 20, 50, and 100 atomic % Yb:YAG. The maximum line locates at about 2θ of 33.4°. The relative intensity of the peak at 2θ of 18° is about 20%. Apparent structural changes can be found in Figure 2 by comparing them with each other. Typically the relative intensities of two peaks at about 27.8° and 29.6° are seen. The change is dependent on the doped Yb^{3+} molar ratio from 10% and 20% to 50% and then 100% Yb:YAG.

The 2θ angle position change of the maximum line (420) of four Yb-doped YAG powders is shown in Figure 3. They are $K\alpha_1$ X-ray peaks, and $K\alpha_2$ peaks were stripped. Hence, the cell constants calculated from Figure 3 are 12.023, 11.991, 11.988, and 11.960 Å for 10, 20, 50, and 100 atomic % doped Yb:YAG, separately. These values are greater than what theoretically they should be (a = 11.931 Å for YbAG, JCPDS[28] No. 73-1369, and a = 12.01 Å for YAG, JCPDS No.33-40; thus, we know the cell constant of Yb:YAG lies between 11.931 and 12.01 Å). The reason may be caused by the

(10) Patel, F. D.; Honea, E. C.; et al. *IEEE J. Quantum Elect.* **2001**, *37* (1), 135.
(11) Shimada, T.; Ishida, Y.; et al. *Opt. Commun.* **2001**, *194*, 238.
(12) Spühler, G. J.; Paschotta, R.; et al. *Appl. Phys. B* **2001**, *72*, 285.
(13) Raghavan, R. S. *Phys. Rev. Lett.* **1997**, *78*, 3618.
(14) Guerassimova, N.; Garnier, N.; et al. *Chem. Phys. Lett.* **2001**, *339*, 197.
(15) Antonini, P.; Belogurov, S.; et al. *Nucl. Instrum. Methods Phys. Res. A* **2002**, *486*, 799−802.
(16) Antonini, P.; Belogurov, S.; et al. *Nucl. Instrum. Methods Phys. Res. A* **2002**, *488*, 591−603.
(17) Saikawa, J.; Kurimura, S.; et al. *Opt. Mater.* **2002**, *19*, 169−174.
(18) Qiu, H.; Yang, P.; et al. *Mater. Lett.* **2002**, *55*, 1−7.
(19) Zhou, Y.; Thai, Q.; et al. *Opt. Commun.* **2003**, *219*, 365−367.
(20) Manalert, R.; Rahaman, M. N. *J. Mater. Sci.* **1996**, *31* (13), 3453.
(21) Paz Vaqueiro, M.; López-Quintela, A. *J. Mater. Chem.* **1998**, *8* (1), 161.
(22) Veith, M.; Mathur, S.; et al. *J. Mater. Chem.* **1999**, *9* (12), 3069.
(23) Wang, H. M.; Simmonds, M. C.; Rodenburg, J. M. *Mater. Chem. Phys.* **2003**, *77*, 802−807.
(24) Avrami, M. *J. Chem. Phys.* **1940**, *8*, 212.
(25) Avrami, M. *J. Chem. Phys.* **1941**, *9*, 177.
(26) Marotta, A.; Buri, A.; Valenti, G. L. *J. Mater. Sci.* **1978**, *13*, 2483.
(27) Znidarsic, V.; Kolar, P. O. *J. Mater. Sci.* **1991**, *26*, 2490.
(28) PCPDFWIN, Version 2.1, JCPDS ICDD International Centre for diffraction Data, June 2000.

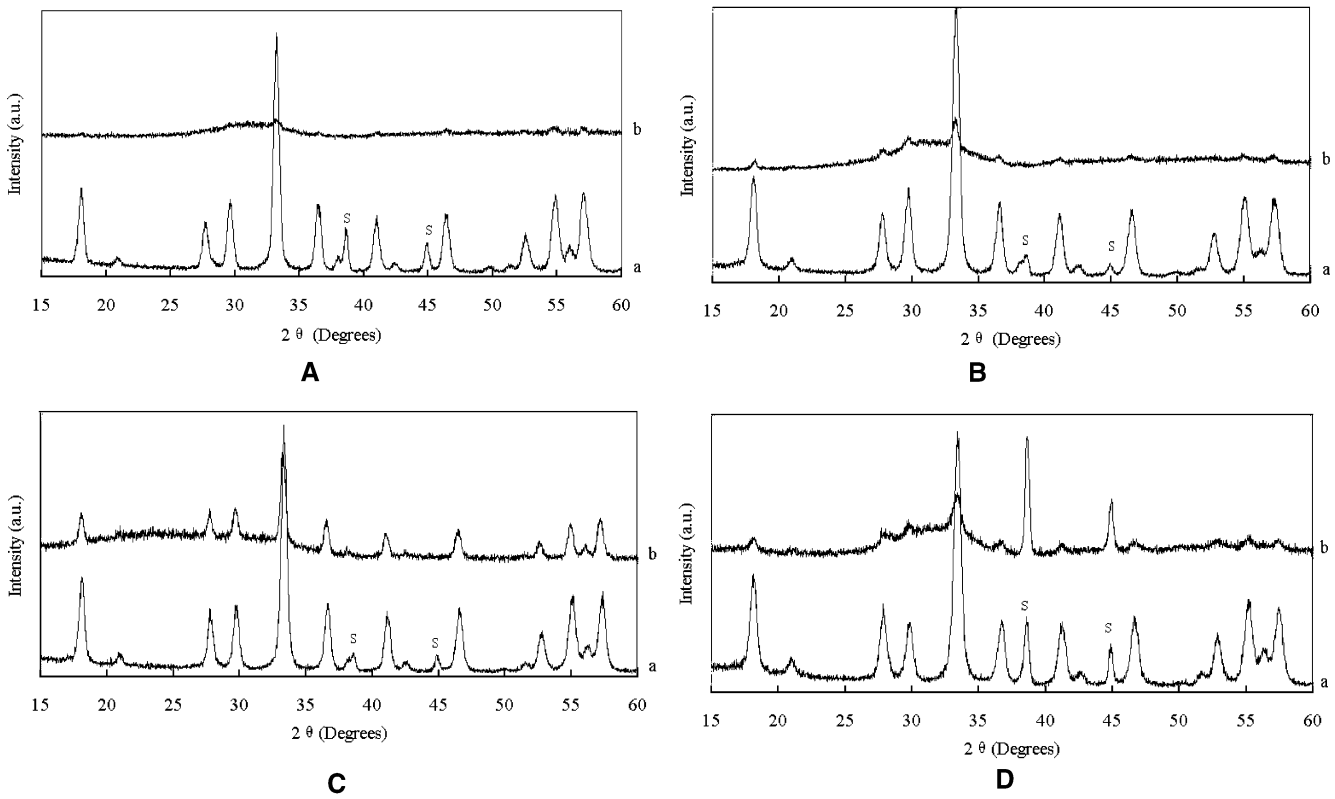

Figure 2. XRD patterns of Yb:YAG powders: (A) 10 atomic %; (B) 20 atomic %; (C) 50 atomic %; (D) 100 atomic %.

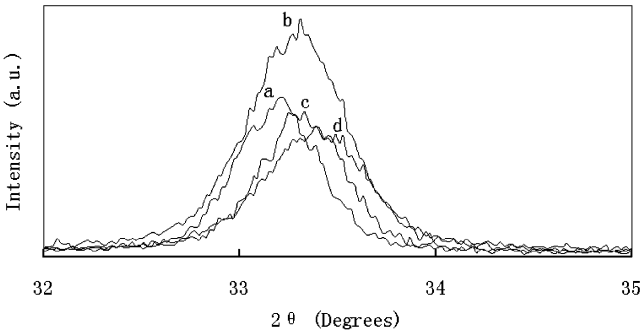

Figure 3. XRD peaks at about 33.5° (420) of the Yb-doped YAG: (a) 10 atomic %; (b) 20 atomic %; (3) 50 atomic %; (d) 100 atomic %.

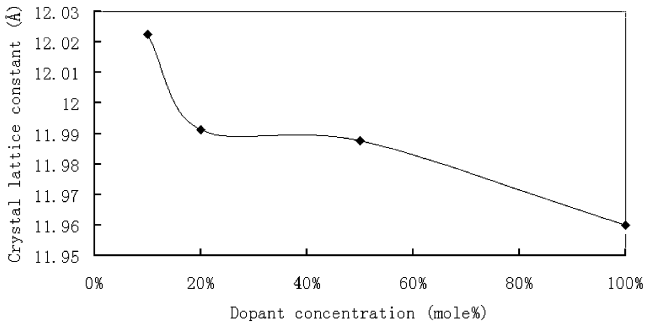

Figure 4. Plot of the lattice constant with Yb doping concentrations in YAG.

powder consisting of nanoparticles, which results in the lattice expansion.[29,30] Thus, with the increase in time or temperature of the calcination, the cell lattice will become close to the theoretical value as the particle size increases. The relationship between the lattice parameters and the Yb concentration then is shown in Figure 4. It does not present the linear relationship. Because the effective radius of Yb^{3+} (0.86)[31] is smaller than that of Y^{3+} (0.89), doping Yb into YAG garnets will decrease the crystal lattice constant and lead to the structure deformation. When the Yb^{3+} doping concentration is below 20 atomic %, the lattice constant decreases sharply. However, there is almost no change of the lattice constant between the doping concentrations of 20 and 50 atomic %. Then, the lattice constant decreases smoothly again from 50 to 100 atomic %. Clearly, these changes are dominated by the distribution of the occupied positions of Yb^{3+} in YAG.

3.1.2. Typical XRD patterns of 100 atomic % Yb:YAG thin films on Si substrates that were heated at 850 °C for various times are shown in Figure 5. A structure composed of very fine nanocrystallites and an amorphous phase are observed (850 °C for 1 h). Only a single phase (garnet) is shown in Figure 5. The intensities of all peaks increased with the increment in the calcination time until they reached a saturation level. When the peak intensities of thin film XRD patterns at various heat-treatment conditions are compared, e.g., the thin film sample at 850 °C for 23 h in Figure 5 to that of the powder XRD patterns in Figure 2, it was found that the crystal growth in thin films exhibits highly preferred orientation growth. Especially, it is seen that the relative intensity of the (211) peak at 2θ of about 18° is enhanced from 45% at 850 °C for 1 h of calcination to 85% at 850 °C for 23 h of heat treatment. This percentage value is much higher than about 20% for powders heated at 850 °C for 11 h: 37.24% for YAG (JCPDS[28]

(29) Ayyub, P.; Multani, M.; et al. *J. Phys. C: Solid State Phys.* **1988**, *21*, 2229.
(30) Lamber, R.; Wetjen, S.; Jaeger, N. I. *Phys. Rev. B* **1995**, *51*, 10968.
(31) Klein & Hulburt, *Manual of Mineralogy*, 20th ed.; 1985.

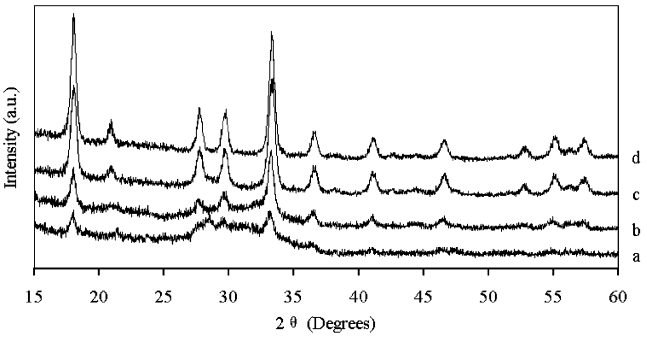

Figure 5. XRD patterns of 100 atomic % Yb-doped YAG thin films on Si. Heat treatment at 850 °C: (a) 1 h; (b) 3 h; (c) 8 h; (d) 23 h.

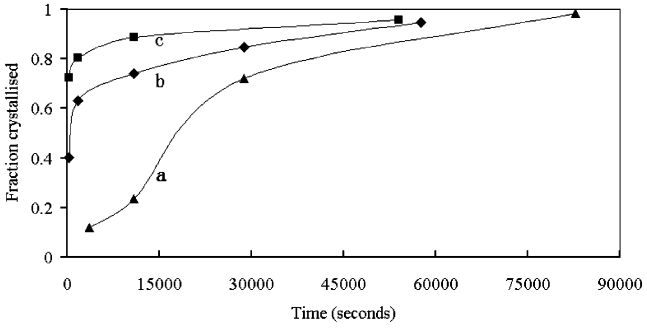

Figure 6. Combined plot of the crystallized fracture via the change of time for 100 atomic % Yb:YAG thin films: (a) 850 °C; (b) 900 °C; (c) 950 °C.

No. 33-40) and 65.37% for YbAG (JCPDS No. 73-1369). The same result of the preferred orientation of Yb:YAG was found at other heating temperatures. An unknown peak at 2θ of 16.9° shown in the initial stage is due to the fast heating rate, but it disappeared upon further calcination. Hence, the texture maximum is the (211) peak, which can be used to stand for the amount or degree of thin film crystallization.

3.2. Activation Energy of Crystalline Growth in the Thin Films. The Johnson−Mehl−Avrami equation, shown below, was used to model the isothermal growth data.[24−27]

$$x(t) = 1 - \exp[-(kt)^n] \quad (1)$$

It can be rearranged as

$$\ln \ln[1 - x(t)]^{-1} = n \ln k + n \ln t \quad (2)$$

where $x(t)$ is the volume fraction of the transformed phase, t the heating time, and n a morphology index, which is related to the crystallization mechanism, and k could follow as the Arrhenius equation

$$k(T) = k_0 \exp(-E_a/RT) \quad (3)$$

Thus,

$$\ln k = \ln k_0 - E_a/RT \quad (4)$$

where k_0 is a constant, T is the temperature, R is the gas constant (8.314 J mol^{-1}), and E_a is the activation energy associated with nucleation and growth. Figure 6 shows the results corresponding to the isothermal growth experiments at 850, 900, and 950 °C. The figure was built up as follows. The integrated intensity of the

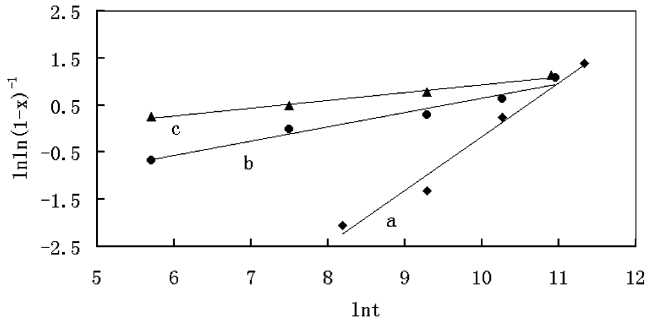

Figure 7. Plot of ln ln$(1 - x)^{-1}$ versus ln(t) of 100% Yb:YAG thin films: (a) 850 °C; (b) 900 °C; (c) 950 °C.

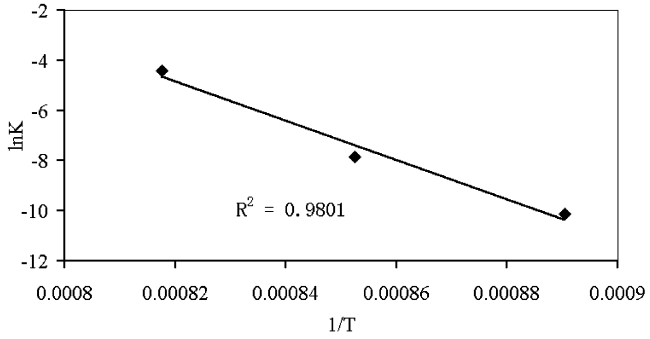

Figure 8. Relationship curve of ln K and 1/T of 100 atomic % Yb:YAG thin films.

texture maximum (211) in the XRD patterns increased until they reached a saturation level. The integrated intensity of the (211) peak, normalized to this saturation value, was used to monitor the crystalline fraction of the film, $x(t)$. Thus, each curve point corresponds to the integrated intensity of the (211) line, at that time and temperature, divided by the saturation value. Here, it should be reasonable that we use the integrated intensity of the texture maximum (211) because it increased much faster than other increased peaks in XRD patterns with the increment in the calcination time and, on the other hand, we do no expect any sintering to occur under the relatively low calcination temperatures used here.

Linear regression analysis of the plots ln ln$[1 - x(t)]^{-1}$ versus ln(t) according to eq 2 is shown in Figure 7. We can obtain three rate constants by the three intercepts with the vertical axis of the plots. Using eq 4, the relationship of ln K and T^{-1} is shown in Figure 8. The correlation coefficient is 0.98. From the slope of the line, the activation energy can be calculated as 653 ± 10 kJ/mol. Other parameters such as the Avrami exponent n and the reaction rate k are all tabulated in Table 1. Within the framework of a proposed classification of diffusion-controlled transformations,[32] an exponent n greater than 2 indicates that the transformation is nucleation limited. The activation energy can be related to nucleation energy. In contrast, values of n of less than 1 indicate that the crystal growth dominates. The average exponent n calculated from our experiments is 0.5379, and this indicates that the crystal growth dominates. However, three values of exponents are dispersion. Especially, at 850 °C the exponent value n is 1.1428 greater than 1. This means that the mechanism of crystallization at this temperature could be

(32) Rao, C.; Rao, K. *Phase transformation in solids;* W & J Mackay Ltd.: Chatham, U.K., 1978.

Table 1. Crystallization Kinetics Parameters for 100% Yb:YAG Films

sample	*n*	*k*	k_0	E_a (kJ/mol)
100% Yb-doped YAG garnet films	850 °C, 1.1428	3.93×10^{-5}	8.03×10^{25}	653 ± 10
	900 °C, 0.3029	3.87×10^{-4}		
	950 °C, 0.168	1.23×10^{-2}		
	average: 0.5379			

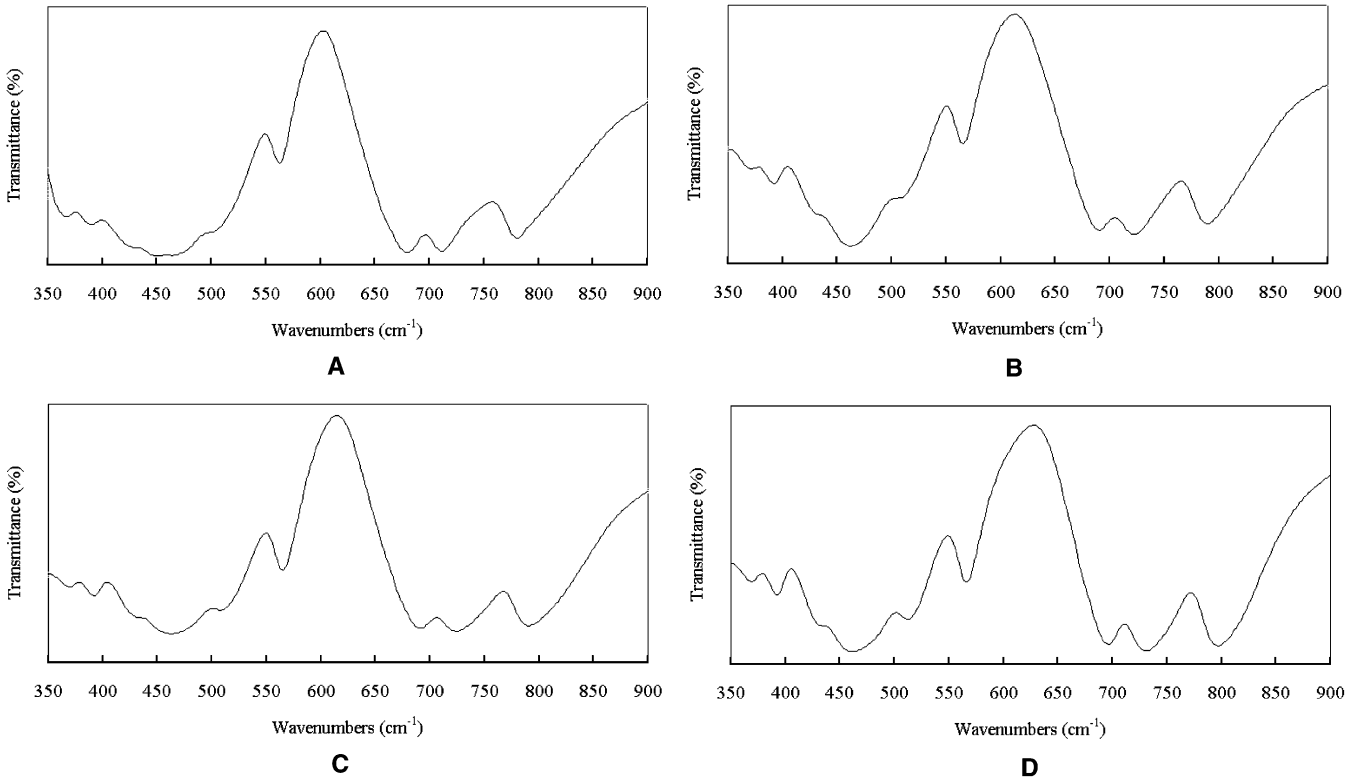

Figure 9. Infrared spectra of Yb-doped YAG powders: (A) 10 atomic %; (B) 20 atomic %; (C) 50 atomic %; (D) 100 atomic %.

nucleation together with the crystal growth limitation. At high temperature, overcoming the nucleation barrier becomes easier. This conclusion is in agreement with our experimental observations by XRD that show a very fast nucleation at the initial stage at high-temperature heat treatment. The results of this part of the work are very close to the studies of crystallization kinetics reported by Johnson and Kriven[33] recently. However, Johnson and Kriven used the sample that was prepared by the rapidly (at approximately 250 °C/s) quenched YAG glass beads from a melting temperature of 2200 °C. The crystallization kinetics was carried out by using differential thermal analysis exotherms. The YAG composition glass beads were populated by the nanoscale crystals of YAG. The material crystallized directly into stoichiometric YAG at temperatures as low as 840 °C. The nanoscale crystals in the glass beads are studied most likely as seeds for subsequent crystal growth. Their obtained activation energy for crystallization was 437 kJ/mol. In general, crystallization in thin films has a higher activation energy than that in bulk materials.

3.3. FT-IR and Raman Spectra. IR transmittance spectra of Yb-doped YAG powders are shown in Figure 9A−D. They are in very good agreement with rare-earth aluminum garnets.[34] A comparison of the IR spectra of the Yb-doped YAG is given in Table 2. There are not any other phase infrared vibration peaks in the IR spectra apart from aluminum garnets (e.g., Y_2O_3, Yb_2O_3, Al_2O_3, or $YAlO_3$). In Table 2, the peak at ~566 cm^{-1} is relatively stable and some other peaks will shift according to the Yb-doped concentration in the YAG matrix. The wavenumber shift value is very small between 20 and 50 atomic % Yb: YAG garnets (e.g., 790 → 790, 723 → 725, and 690 → 692 cm^{-1}). However, the wavenumber change is relatively large from 10 to 20 atomic % and from 50 to 100 atomic % Yb:YAG (e.g., 781 → 790 and 790 → 798 cm^{-1}). The changing tendency is in agree-

Table 2. Comparison of IR Vibrational Frequencies of the Yb:YAG Powders

Yb:YAG				
10%	20%	50%	100%	ref data[34]
781	790	790	798	794
711	723	725	732	726
680	690	692	698	691
563	566	566	566	567
				532
501	510	510	513	522
458	462	462	462	463
428	430	430	430	432
390	392	392	392	396

(33) Johnson, B. R.; Kriven, W. M. *J. Mater. Res.* **2001**, *16*, 1795−1805.

(34) Hofmeister, A. M.; Campbell, K. R. *J. Appl. Phys.* **1992**, *72*, 638.

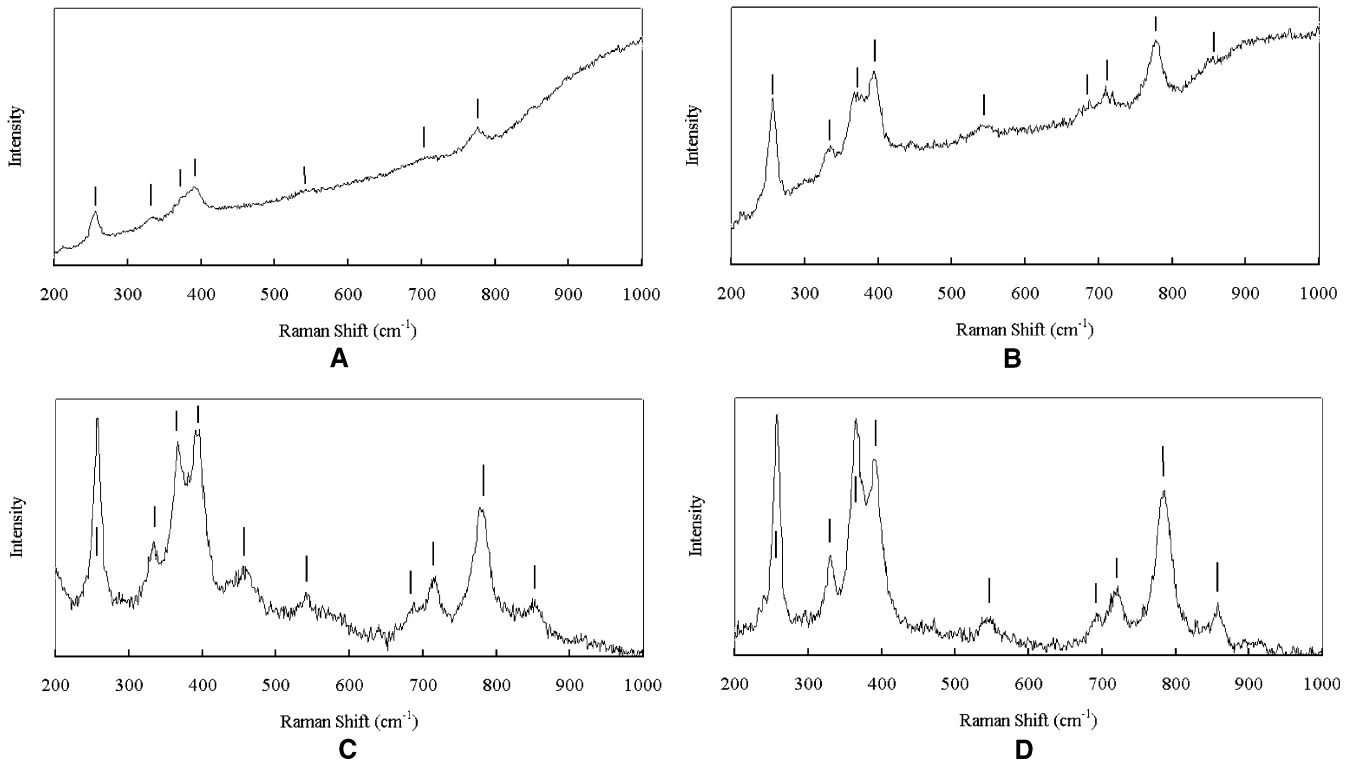

Figure 10. Raman spectra of Yb-doped YAG powders: (a) 10 atomic %; (b) 20 atomic %; (c) 50 atomic %; (d) 100 atomic %.

Table 3. Comparison of Raman Active Vibrational Frequencies of the Yb-Doped YAG Powders

10%	20%	50%	100%
	850	850	857
777	778	779	785
712	713	714	720
	688	689	695
541	541	542	548
		459	
391	394	393	390
372	368	366	365
335	335	333	330
256	257	257	258

ment with the lattice deformation we discussed in section 3.1.1.

Raman spectra of Yb-doped YbAG powders are shown in Figure 10a−d: (i) 7 Raman active vibrational modes are observed in Figure 10a for 10 atomic % Yb:YAG particles; (ii) 9 Raman active vibrational modes are found in Figure 10b for 20 atomic % Yb:YAG particles; (iii) 10 Raman modes are observed in Figure 10c for 50 atomic % Yb:YAG particles; (iv) 9 Raman modes can be seen in Figure 10d for 100 atomic % Yb:YAG particles, which are all indicated by the vertical solid line in the figures. A comparison of Raman vibrational frequencies of the Yb-doped YAG powders is given in Table 3. The lines of the observed Raman active vibrational modes are in good agreement with the experimental and calculated Raman mode frequencies of YAG or rare-earth aluminum garnets.[35,36] Some frequency and intensity changes of the Raman vibrational lines are found. The changing tendency presents the same way with the IR spectra and the cell constant. For instance,

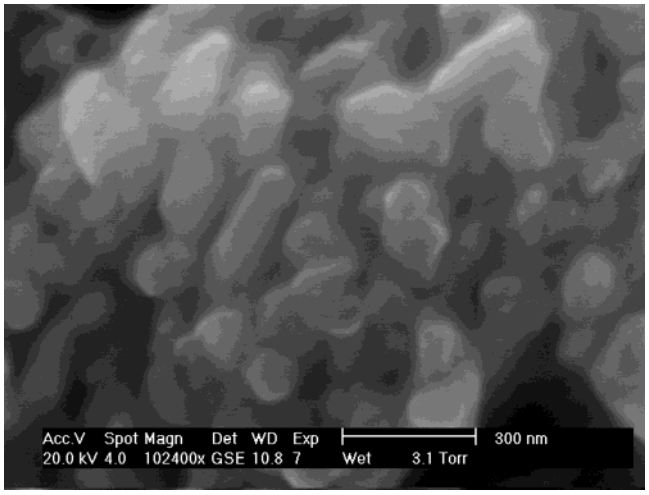

Figure 11. Typical scanning electron micrographs of Yb-doped YAG powders.

the frequency of the line, which is at 711 cm^{-1} for 10 atomic % Yb:YAG particles, increases to almost the same 723 and 725 cm^{-1} at 20 and 50 atomic % Yb:YAG powders (Figure 10b,c) and then becomes 732 cm^{-1} in 100 atomic % Yb:YAG powders (Figure 10d). Especially, a distinctive change can be observed in the comparison of the relative intensities of the two lines, the frequencies of which are located at about 365 and 390 cm^{-1}. The intensity of the line at about 365 cm^{-1} is smaller than that of the line at about 390 cm^{-1} in the former three samples (Figure 10a−c). However, the intensity of the line at 365 cm^{-1} becomes greater than that of the line at 390 cm^{-1} for 100 atomic % Yb:YAG.

The structural changing tendency is now confirmed again by the observed Raman spectra. This explains that the doped Yb^{3+} affects the lattice vibration modes, which is related to the doping concentration and the

(35) Hurrell, J. P.; Porto, S. P. S.; et al. *Phys. Rev.* **1968**, *173*, 851.
(36) Papagelis, K.; Kanellis, G.; et al. *Phys. Status Solidi B* **2001**, *223*, 343−347.

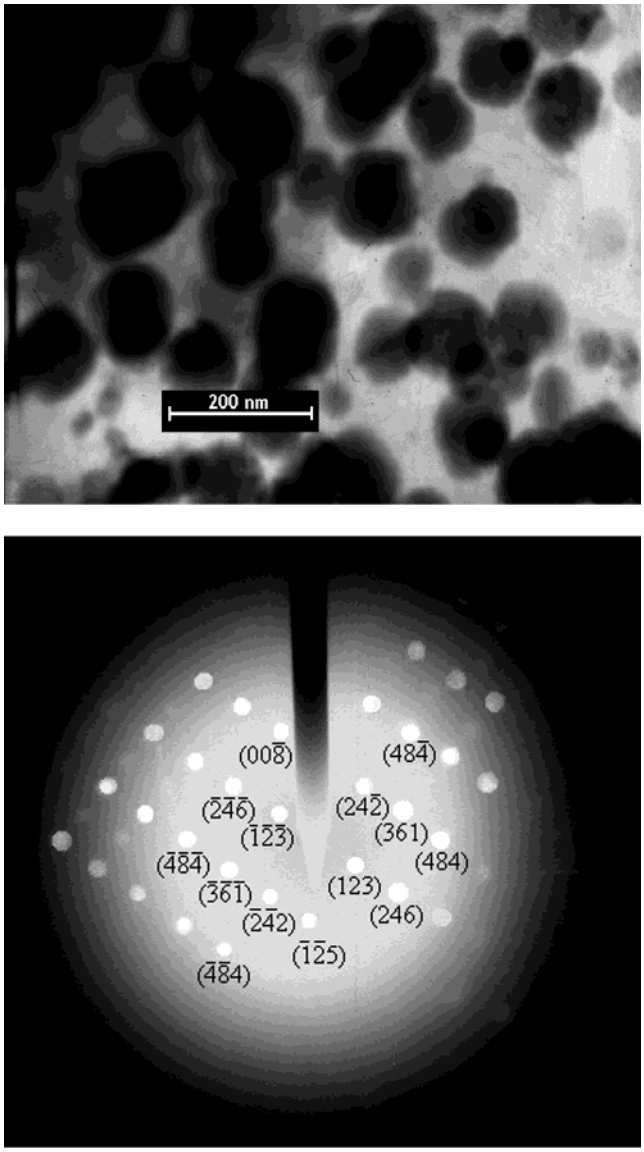

Figure 12. (a) Bright-field transmission electron image of Yb-doped YAG powders. (b) Micro area electron diffraction pattern of Yb:YAG crystals.

distribution of the occupied positions of Yb^{3+} cations in the garnet structure. However, this change could be divided into three circumstances according to the doping concentration of Yb^{3+}, i.e., 1−20, 20−50, and 50−100 atomic %. The changes of lattice vibrations will influence the interaction between the Yb^{3+} ion and the host YAG. These changes will at last have some effect on the spectra and the laser and scintillation performance of Yb:YAG materials. This could be one of the causes why these materials present better laser and scintillation properties that have been studied by many researchers[12,16,17] in about 20 atomic % Yb:YAG crystals.

3.4. Morphologies of Nanosized Yb-Doped YAG Powders. A typical scanning electron micrograph of Yb-doped YAG powders is shown in Figure 11. The morphologies of various concentrations of Yb-doped YAG are the same and show no differences with the change of the Yb-doped concentration in YAG. It can be observed that the particles do not have very regular shape. They exhibit generally lengthened, rounded irregular shape. Some particles are aggregated but mainly are still dispersed. The particle size is well distributed, and the uniform size is about 100 nm.

A bright-field TEM image of Yb-doped YAG is shown in Figure 12a. A micro area electron diffraction pattern of a Yb:YAG crystal is shown in Figure 12b, correspondingly. The shape and size of the particles are the same as those with the results of the scanning electron micrograph. The diffraction patterns were identified as the garnet structure. The corresponding crystal plane indexes were all labeled in the picture. The axis of the zone is of the indice [$\bar{2}$, 1, 0].

4. Conclusions

Powders and thin films of Yb-doped YAG with nanosized crystallites were prepared by sol−gel methods at significantly lower temperature than the traditional method. The crystal transformation in thin films on Si(100) shows a strong preferred texture (211) growth. The crystallization kinetics was studied by the Avrami model, and the activation energy was 653 ± 10 kJ/mol. The crystallization mechanism is mainly dominated by the crystal growth. The studies of XRD, IR, and Raman spectra of Yb:YAG with various doped concentrations show the crystal lattice deformation, and the phonon vibration changes according to the Yb^{3+}-doped concentration in YAG, which could be divided into three ranges of Yb^{3+} mole concentration (i.e., 1−20, 20−50, and 50−100 atomic %). This could, in part, explain why about 20 atomic % Yb:YAG crystals generally present the better laser and scintillation properties that have been studied by many other researchers.

Acknowledgment. H.M.W. acknowledges the help of Dr. Christopher Sammon in MRI of Sheffield Hallam University to finish the Raman spectra experiments.

CM021248L